Protonation of Propene on Silica-Grafted Hydroxylated Molybdenum and Tungsten Oxide Metathesis Catalysts: A DFT Study

Ghashghaee, Mohammad

Department of Process Design and Construction, Faculty of Petrochemicals, Iran Polymer and Petrochemical Institute, P.O. Box 14975-112, Tehran, I.R. IRAN

Ghambarian, Mehdi*[+]

Gas Conversion Department, Faculty of Petrochemicals, Iran Polymer and Petrochemical Institute, P.O. Box 14975-112 Tehran, I.R. IRAN

ABSTRACT: *Theoretical assessment of the protonation reaction in the activation of propene on hydroxylated Mo(VI) and W(VI) metathesis catalysts is presented in this paper using the density functional theory calculations and five support clusters varying from simple SiO_4H_3 clusters to a large $Si_4O_{13}H_9$ cluster. The bond distances and thermochemical data were similar for most of the clusters. The formation of isopropoxide was more favorable than a propoxide counterpart bonded via the primary carbon atom, with the Gibbs free energies of –3.73 and –7.78 kcal/mol, respectively, for the W catalyst. Overall, the 1T cluster models with optimized H atoms or an all-relaxed alternative would be considered appropriate replacements for a larger 4T cluster model saturated with OH groups and optimized terminal hydrogen atoms. The largest deviations in the energetic data were observed between the protonated structures formed on the two larger clusters saturated with either OH or H groups.*

KEYWORDS: *Metathesis; Propene; Density functional theory; Tungsten; Molybdenum; Protonation; Activation; Silica.*

INTRODUCTION

Ethene, propene, and butene are the three most important monomers to the polymer industries [1-8]. However, the balanced supply of these alkenes in the market has entailed the development of interconversion technologies, such as the alkenes metathesis [9-10]. Monolayer metal oxides involving, e.g., W and Mo, anchored to porous supports are efficient metathesis catalysts [11]. In heterogeneous catalysis, metal–alkylidene species are inevitably formed from adsorbed alkene molecules and operate until consumption in some unfavorable reactions [12]. Further studies are still necessary to shed light on the exact nature and structural description of the active sites in connection with the type and acid functionality of the inorganic support, however [12-13].

***** *To whom correspondence should be addressed.*
+ E-mail: m.ghambarian@ippi.ac.ir
1021-9986/2019/6/175-187 13/$/6.03

The quantum chemical calculations are helpful in this regard as standard complementary tools for the identification of the reaction pathways and studying the well-defined catalysts [14]. Therefore, several theoretical studies [15-17] have appeared on the reaction pathways and the identification of the initial active sites in MoO_3/γ-Al_2O_3, MoO_3/SiO_2 and MoO_3/HZSM-5 pre-catalysts. Much fewer studies addressed a tungsten-based active sites, e.g., in a model W/ZSM-5 catalyst [18]. Recently, Amakawa et al. [13, 19-21] combined the operando infrared spectroscopy technique with microcalorimetry and (propene) reactivity studies over the MoO_x/SBA-15 catalyst using isotopic labeling to trace the genesis of carbene species. The DRIFT spectrum of MoO_x/SBA-15 material has clearly proven the presence of molybdenol (Mo–OH) groups on the surface as the pre-catalyst [13]. It is noteworthy, however, that the preferable active metathesis catalysts in industrial practice are based on WO_3 and those involving MoO_3 and Re_2O_7 are employed limitedly [22-23]. According to the new mechanism, the active site formation starts with the protonation of propene (propylene) to form surface Mo(VI)–isopropoxide species driven by the effect of surface Brønsted acidity. As a first molecular modeling attempt, this paper deals with the energetics, partial charges, and geometrical properties of the initially formed propoxide stabilized on single-atomic W and Mo sites grafted onto five model nanoclusters of the meso-structured silica.

COMPUTATIONAL METHOD

The cluster models of silica were taken from the established crystallographic data for beta cristobalite [24]. This ordered material is known as the best representative model for the cluster modeling of mesoporous silica materials, which has been employed in several previous studies [25-30]. Five cluster models of the meso-structured silica were investigated: (A1) a small (1T) all-fixed silica support, (A2) an alternative small cluster with optimized hydrogen atoms, (A3) an all-relaxed alternative of the first cluster, (A4) a larger (4T) silica support saturated with optimized hydrogen atoms at the boundaries, and (A5) an adequately large (4T) nanocluster saturated with hydroxyl groups in which the terminal hydrogen atoms were optimized. All broken bonds at the boundaries of the A2, A4, and A5 silica clusters were terminated by hydrogen atoms placed in the same direction as expected in a real crystal for the next removed T atom. As such, the size of the inorganic ligand varied from a simple SiO_4H_3 cluster to an adequately large $Si_4O_{13}H_9$ cluster. The molecular calculations were implemented by N.W. Chem. 6.5 [31] and Multiwfn 3.3.8 [32]. The graphical outputs were generated by Mercury 3.3 [33]. The molecular modeling of the pre-catalyst was implemenbted by the stabilization of single-atomic hydroxylated Mo and W species with a +6 oxidation state as identified earlier [13] on the surface of the mentioned supports. The obtained structures were labeled as A1Mo–A5Mo and A1W–A5W, respectively. Next, the protonated structures were simulated in two binding modes, which involved the attachment to either the primary or secondary carbon atoms of propene. The resulting structures were labeled as B1Mo–B5Mo and C1Mo–C5Mo, respectively, for the case of molybdena catalyst. The corresponding structures with W were named B1W–B5W and C1W–C5W. In addition to the organic part and Mo/W species, the bridging oxygen atoms were also relaxed.

All of the calculations were implemented using the hybrid functional of M06 [34] coupled with the Def2-TZVP [35] basis set. This level of theory is considered to be suitable for the transition metal-exchanged materials [36-38]. The same computational method was applied to estimate the highest occupied and lowest unoccupied molecular orbital (HOMO and LUMO) energy levels of the optimized structures within the framework of the Frontier Molecular Orbital (FMO) theory [39]. The partial charges were calculated based on the Natural Bond Orbital (NBO) population [40] at the same level of theory. The Gibbs free energy change of protonation (ΔG) was calculated from the corresponding enthalpy (ΔH) and entropy changes (ΔS) according to the fundamental equation ($\Delta G = \Delta H - T\Delta S$), all estimated for the following reactions.

$$[SiO_2]-OM(O_2)OH + CH_2CHCH_3 \rightarrow [SiO_2]-OM(O_2)OCH_2CH_2CH_3 \quad (1)$$

$$[SiO_2]-OM(O_2)OH + CH_2CHCH_3 \rightarrow [SiO_2]-OM(O_2)O(CH_3)CHCH_3 \quad (2)$$

in which M is either Mo(VI) or W(VI).

RESULTS AND DISCUSSION

As was pointed out previously, the latest state of knowledge on the activation of heterogeneous metathesis catalysts suggests the formation of a protonated intermediate from olefin at the beginning step. The experimental evidences were collected on acidic molybdenum catalysts with propene as the feedstock. In the present study, total of 30 clusters were optimized. The optimized geometries are shown in Fig. S1. As apparent, most of the optimized geometries were similar for both Mo and W catalysts.

The energetic data for the protonation reactions represented by Eq. (1) and (2) for the protonated propene species with primary and secondary carbon atoms are shown in Table S1. In terms of thermodynamic, the protonated structures were more stable than the corresponding precatalysts. The obtained data predicted that the energetics of the molybdenum and tungsten catalysts were very similar within the accuracy of the calculations. The largest deviations in the thermodynamic changes were observed between the protonated structures formed on A4 and A5 supports. This indicates that the A4 silica cluster is the least appropriate choice in terms of thermochemistry. The formation of the alkoxide intermediates was accompanied by an expected decrease in entropy, lying in the range of –0.05 to –0.03 kcal/(mol.K). For both of the catalysts, the formation of the isopropoxide species was more favorable than the corresponding structure involving a primary carbon atom attachment: compare, e.g., the ΔG values of –3.74 and –7.78 kcal/mol, respectively, for the B5W and C5W protonated structures. Correspondingly, the protonation enthalpies were –13.88 and –18.29 kcal/mol, respectively.

Tables S2 and S3 show the geometrical parameters of the silica-grafted Mo and W species, respectively. The tables also contain the corresponding data for the protonated clusters. The Mo–O1 and Mo–O4 distances varied in the ranges of 1.86–1.88 Å and 1.85–1.87 Å, respectively. Whereas the O4–C1 distance in the B series of products was equal to 1.41 Å, the corresponding values (O4–C2) in the C series of products were by 0.01–0.02 Å longer. Moreover, the initial Brønsted acidic O–H distances were 0.96–0.97 Å. The same bond lengths were observed in the case of W catalysts. However, the W–O–C interbond angles were on average by 4.23° larger than those of Mo–O–C. It was also evident that the lowest M–O–C angle on both of the catalysts belonged to the products formed on the A5Mo and A5W clusters.

The results of the NBO analysis are listed in Tables S4 and S5, respectively, for the Mo and W catalysts. As anticipated, the carbon atoms attached to the bridging O atom were less negatively charged: while the charge on C1 in the propoxide species bonding through a primary carbon atom was only slightly negative, the charge on C2 in the secondary counterpart was positively charged. Among the O atoms, the bridging oxygen atoms (O1 and O4) carried more negative charges than those in the dioxo ligand (O2 and O3) as expected from their numbers of coordination. As evident, all of the charges on the O atoms of the Mo-containing clusters were slightly less negative than those on the W-containing counterparts. For instance, the average partial charges on O2 and O3 were –0.483 and –0.595 e for the Mo and W series. Analogously, the average partial charge on the initial metal center was +1.612 and +1.906 e for Mo and W. Although the partial charge on the M(VI) center was far from the nominal charge of +6, the partial charges on all of the Mo clusters were slightly smaller than those of W-containing structures. The positive charge of proton on the initial pre-catalyst was found to be +0.506 and +0.510 e for the silica-supported Mo and W sites, which is almost half the formal charge of the free protons. On the other hand, the total charge of the protonated hydrocarbon segment was +0.330 and +0.342 e for the Mo and W catalysts. The largest changes in the partial charge of oxygen atoms belonged to O4, with the decrease in its negative charge upon protonation. These altogether indicated that the total positive charge on the hydrocarbon segment was reduced upon protonation owing to the partial flow of electrons from O4 to this segment and less partially to the metal center.

As a comparative remark on the choice of a cluster model to ascertain a realistic representation of the silica surface, the A5Mo and A5W clusters may be taken as the most appropriate models of the surface. The corresponding protonated structures (B5Mo, C5Mo, B5W, and C5W) can also be considered as reference computational models for comparison with simpler geometries. In terms of the energetic data, the 4T silica support saturated with optimized hydrogen atoms at the boundaries followed by the 1T all-fixed cluster showed the highest deviations from the results of the reference cases. Although

the M–O–C angles in the reference cases were smaller than the rest of clusters, the bond distances were almost similar for all of the support variants. Regarding the NBO charges, more disparate data were observed. Within the acceptable ranges, however, one may consider the results over the five silica clusters comparable. In summary, the 1T clusters with optimized hydrogen atoms or an all-relaxed alternative can be used in place of the reference cluster for the investigated system in a less demanding computational framework without much inaccuracy with the computational results. For instance, the protonation enthalpies of the formation of isopropoxide on the above-mentioned support clusters for both of the catalysts agreed within 3%.

Tables S6 and S7 contain the molecular orbital (HOMO and LUMO) energy levels and the energy gaps of the optimized clusters. From these data, chemical hardness defined as $\eta = (E_{LUMO} - E_{HOMO})/2$ [41] can be calculated for the assessment of reactivity of the clusters [27-28]. According to this criterion, the reactivity of the Mo-containing clusters was slightly (by 0.32 eV on average) higher than that of W-containing structures, due mainly to the relatively (by 0.71 eV on average) more stable LUMO levels in the formers. However, the protonation of propene led to almost no changes in either the frontier molecular orbital energy levels or the $\Delta E_{HOMO-LUMO}$ on both of the catalysts. The spatial distributions of selected molecular orbitals are shown in Fig. S2. While HOMOs showed regions of high density around the metal center in most of the cases, LUMOs were more or less delocalized over the silica support. The HOMO molecular orbitals also indicated pronounced π^* interactions in the M=O bonds. Upon protonation, these HOMO interactions were slightly delocalized and drawn toward the hydrocarbon fragment.

CONCLUSIONS

Theoretical evaluations of thermochemical, geometrical, and electronic properties of the silica-supported Mo and W metathesis catalysts were implemented using the cluster modeling approach with five cluster models of the mesoporous silica surface at the M06/Def2-TZVP level of theory. The energetics of the molybdenum and tungsten catalysts were found to be very similar. The formation of the isopropoxide was more favorable than the counterpart attached through the primary carbon atom. Although similar bond lengths were observed on the catalysts, the W–O–C angles were on average by 4.23° larger than those of Mo–O–C where the carbon atoms bonded to the bridging O atom were less negatively charged than other C atoms. The average partial charges on the initial Mo(VI) and W(VI) centers were +1.612 and +1.906 e, respectively. The results of NBO calculations revealed the partial flow of electrons from the bridging O atom to the hydrocarbon segment and to a less extent to the metal center during the activation. The chemical hardness of the W-containing structures was (by 0.32 eV on average) higher than that of Mo-based clusters owing to the relatively (by 0.71 eV on average) higher LUMO levels in the formers. Finally, the 1T cluster models with optimized H atoms or all-relaxed elements turned out to be suitable alternatives to the more demanding 4T cluster saturated with OH groups with optimized terminal hydrogen atoms.

Acknowledgments

The authors gratefully acknowledge the technical assistance of Ms. Mahboobeh Balar.

Received : Jun. 14, 2018 ; Accepted : Sep. 10, 2018

REFERENCES

[1] Ghashghaee M., Shirvani S., Two-step Thermal Cracking of an Extra-Heavy Fuel Oil: Experimental Evaluation, Characterization, and Kinetics, *Ind. Eng. Chem. Res.*, **57** (22): 7421–7430 (2018).

[2] Ghashghaee M., Karimzadeh R., Multivariable Optimization of Thermal Cracking Severity, *Chem. Eng. Res. Des.*, **89** (7): 1067–1077 (2011).

[3] Ghashghaee M., Karimzadeh R., Applicability of Protolytic Mechanism to Steady-State Heterogeneous Dehydrogenation of Ethane Revisited, *Micropor. Mesopor. Mat.*, **170**: 318–330 (2013).

[4] Hajheidary M., Ghashghaee M., Karimzadeh R., Olefins Production from LPG via Dehydrogenative Cracking over Three ZSM-5 Catalysts, *J. Sci. Ind. Res.*, **72** (12): 760–766 (2013).

[5] Karimzadeh R., Ghashghaee M., Design of a Flexible Pilot Plant Reactor for the Steam Cracking Process, *Chem. Eng. Technol.*, **31** (2): 278–286 (2008).

[6] Shirvani S., Ghashghaee M., Combined Effect of Nanoporous Diluent and Steam on Catalytic Upgrading of Fuel Oil to Olefins and Fuels over USY Catalyst, *Petrol. Sci. Technol.*, **36** (11): 750–755 (2018).

[7] Ghashghaee M., Karimzadeh R., Dynamic Modeling and Simulation of Steam Cracking Furnaces, *Chem. Eng. Technol.*, **30** (7): 835–843 (2007).

[8] Sedighi M., Keyvanloo K., Towfighi Darian J., Olefin Production from Heavy Liquid Hydrocarbon Thermal Cracking: Kinetics and Product Distribution, *Iran. J. Chem. Chem. Eng. (IJCCE)*, **29** (4): 135–147 (2010).

[9] Ghashghaee M., Heterogeneous Catalysts for Gas-phase Conversion of Ethylene to Higher Olefins, *Rev. Chem. Eng.*: DOI: 10.1515/revce-2017-0003 (2017).

[10] Ghashghaee M., Farzaneh V., Nanostructured Hydrotalcite-Supported RuBaK Catalyst for Direct Conversion of Ethylene to Propylene, *Russ. J. Appl. Chem.*, **91** (6): 970−974 (2018).

[11] Lwin S., Wachs I.E., Olefin Metathesis by Supported Metal Oxide Catalysts, *ACS Catal.*, **4** (8): 2505–2520 (2014).

[12] Fierro J.L.G., "Metal Oxides: Chemistry and Applications", CRC Press, Taylor & Francis Group, Boca Raton (2006).

[13] Amakawa K., Wrabetz S., Kröhnert J., Tzolova-Müller G., Schlögl R., Trunschke A., In Situ Generation of Active Sites in Olefin Metathesis, *J. Am. Chem. Soc.*, **134** (28): 11462–11473 (2012).

[14] Handzlik J., Kurleto K., Theoretical Investigations of Heterogeneous Olefin Metathesis Catalysts, *Curr. Org. Chem.*, **17** (22): 2796–2813 (2013).

[15] Handzlik J., Sautet P., Structure of Dimeric Molybdenum(VI) Oxide Species on γ-Alumina: A Periodic Density Functional Theory Study, *J. Phys. Chem. C*, **114** (45): 19406–19414 (2010).

[16] Handzlik J., Computational Study of the Properties and Metathesis Activity of Mo Methylidene Species in HZSM-5 Zeolite, *J. Mol. Catal. A-Chem.*, **316**(1–2): 106–111 (2010).

[17] Handzlik J., Ogonowski J., Structure of Isolated Molybdenum(VI) and Molybdenum(IV) Oxide Species on Silica: Periodic and Cluster DFT Studies, *J. Phys. Chem. C*, **116** (9): 5571–5584 (2012).

[18] Maihom T., Probst M., Liktrakul J., A DFT Study of Tungsten–Methylidene Formation on a W/ZSM-5 Zeolite: The Metathesis Active Site, *Chem. Phys. Chem.*, **16** (15): 3334–3339 (2015).

[19] Amakawa K., "Active Site for Propene Metathesis in Silica-Supported Molybdenum Oxide Catalysts", Department of Inorganic Chemistry: Technischen Universität Berlin (2013).

[20] Amakawa K., Kröhnert J., Wrabetz S., Frank B., Hemmann F., Jäger C., Schlögl R., Trunschke A., Active Sites in Olefin Metathesis over Supported Molybdena Catalysts, *Chem. Cat. Chem.*, **7** (24): 4059–4065 (2015).

[21] Amakawa K., Sun L., Guo C., Hävecker M., Kube P., Wachs I.E., Lwin S., Frenkel A.I., Patlolla A., Hermann K., Schlögl R., Trunschke A., How Strain Affects the Reactivity of Surface Metal Oxide Catalysts, *Angew. Chem. Int. Edit.*, **52** (51): 13553–13557 (2013).

[22] Lavrenov A.V., Saifulina L.F., Buluchevskii E.A., Bogdanets E.N., Propylene Production Technology: Today and Tomorrow, *Catal. Ind.*, **7** (3): 175–187 (2015).

[23] Butler J.R., Metathesis Catalyst for Olefin Production, *US Patent*, US20110077444 A1 (2011).

[24] Sindorf D.W., Maciel G.E., Silicon-29 NMR Study of Dehydrated/Rehydrated Silica Gel Using Cross Polarization and Magic-Angle Spinning, *J. Am. Chem. Soc.*, **105** (6): 1487–1493 (1983).

[25] Zhang B., Lu Y., He H., Wang J., Zhang C., Yu Y., Xue L., Experimental and Density Functional Theory Study of the Adsorption of N_2O on Ion-Exchanged ZSM-5: Part II. The Adsorption of N_2O on Main-Group Ion-Exchanged ZSM-5, *J. Environ. Sci.*, **23** (4): 681–686 (2011).

[26] Balar M., Azizi Z., Ghashghaee M., Theoretical Identification of Structural Heterogeneities of Divalent Nickel Active Sites in NiMCM-41 Nanoporous Catalysts, *J. Nanostruct. Chem.*, **6** (4): 365–372 (2016).

[27] Ghashghaee M., Ghambarian M., Azizi Z., Characterization of Extraframework Zn^{2+} Cationic Sites in Silicalite-2: a Computational Study, *Struct. Chem.*, **27** (2): 467–475 (2016).

[28] Ghambarian M., Azizi Z., Ghashghaee M., Diversity of Monomeric Dioxo Chromium Species in Cr/Silicalite-2 Catalysts: A Hybrid Density Functional Study, *Comp. Mater. Sci.*, **118**: 147–154 (2016).

[29] Ghambarian M., Azizi Z., Ghashghaee M., Cluster Modeling and Coordination Structures of Cu^{+} Ions in Al-Incorporated Cu-MEL Catalysts – A Density Functional Theory Study, *J. Mex. Chem. Soc.*, **61** (1): 1–13 (2017).

[30] Ghambarian M., Ghashghaee M., Azizi Z., Coordination and Siting of Cu^{+} Ion Adsorbed into Silicalite-2 Porous Structure: A Density Functional Theory Study, *Phys. Chem. Res.*, **5** (1): 135–152 (2017).

[31] Valiev M., Bylaska E.J., Govind N., Kowalski K., Straatsma T.P., Van Dam H.J.J., Wang D., Nieplocha J., Apra E., Windus T.L., de Jong W.A., NWChem: A Comprehensive and Scalable Open-Source Solution for Large Scale Molecular Simulations, *Comput. Phys. Commun.*, **181** (9): 1477–1489 (2010).

[32] Lu T., Chen F., Multiwfn: A Multifunctional Wavefunction Analyzer, *J. Comput. Chem.*, **33** (5): 580–592 (2012).

[33] Bruno I.J., Cole J.C., Edgington P.R., Kessler M., Macrae C.F., McCabe P., Pearson J., Taylor R., New Software for Searching the Cambridge Structural Database and Visualizing Crystal Structures, *Acta Crystallogr. B*, **58** (3 Part 1): 389–397 (2002).

[34] Zhao Y., Truhlar D.G., The M06 Suite of Density Functionals for Main Group Thermochemistry, Thermochemical Kinetics, Noncovalent Interactions, Excited States, and Transition Elements: Two New Functionals and Systematic Testing of Four M06-Class Functionals and 12 Other Functionals, *Theor. Chem. Acc.*, **120** (1-3): 215–241 (2008).

[35] Feller D., The Role of Databases in Support of Computational Chemistry Calculations, *J. Comput. Chem.*, **17** (13): 1571–1586 (1996).

[36] Yumura T., Yamashita H., Torigoe H., Kobayashi H., Kuroda Y., Site-Specific Xe Additions Into Cu-ZSM-5 Zeolite, *Phys. Chem. Chem. Phys.*, **12** (10): 2392–2400 (2010).

[37] Göltl F., Hafner J., Structure and Properties of Metal-Exchanged Zeolites Studied Using Gradient-Corrected and Hybrid Functionals. I. Structure and Energetics, *J. Chem. Phys.*, **136** (6): 064501-064501–064501-064517 (2012).

[38] Ghashghaee M., Ghambarian M., Methane Adsorption and Hydrogen atom Abstraction at Diatomic Radical Cation Metal oxo Clusters: First-Principles Calculations, *Mol. Simul.*, **44** (10): 850–863 (2018).

[39] Fukui K., Yonezawa T., Shingu H., A Molecular Orbital Theory of Reactivity in Aromatic Hydrocarbons, *J. Chem. Phys.*, **20** (4): 722–725 (1952).

[40] Glendening E., Badenhoop J., Reed A., Carpenter J., Weinhold F., "NBO 3.1", Theoretical Chemistry Institute, University of Wisconsin, Madison, WI: (1996).

[41] Datta D., On Pearson's HSAB Principle, *Inorg. Chem.*, **31** (13): 2797–2800 (1992).

Supplementary Materials

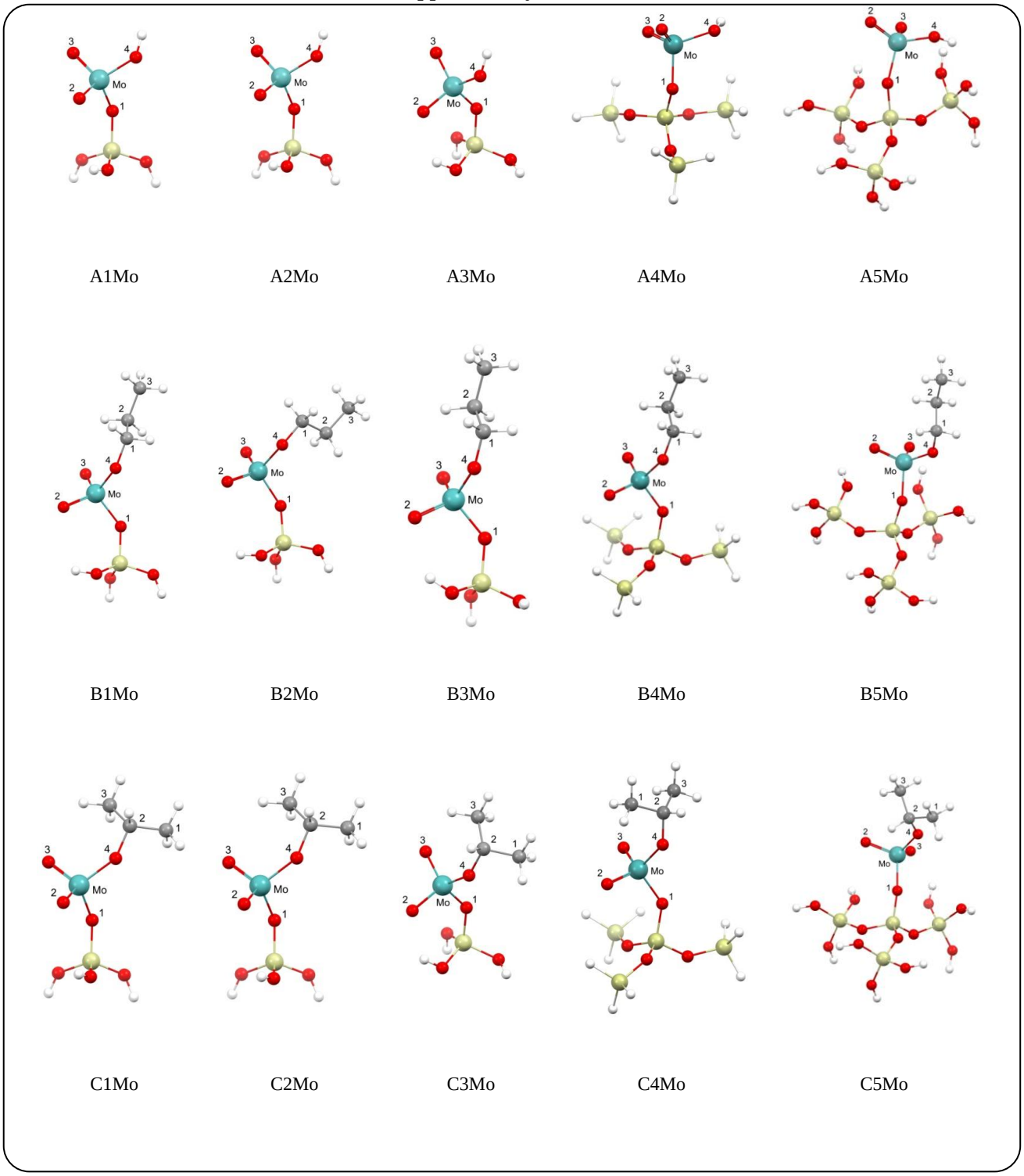

Fig. S1: Optimized geometries of the original precatalyst and the resulting protonated structures after the exposure to propene on different cluster models of MoO_x/SBA-15 and WO_x/SBA-15 catalysts. The darker (red) spheres represent the framework O atoms, the plain (yellow) bigger balls are Si atoms, the plain grey spheres show C atoms, and the small white balls are terminal H atoms. The largest (blue or purple) balls represent Mo or W. Please refer to the online version for references to color.

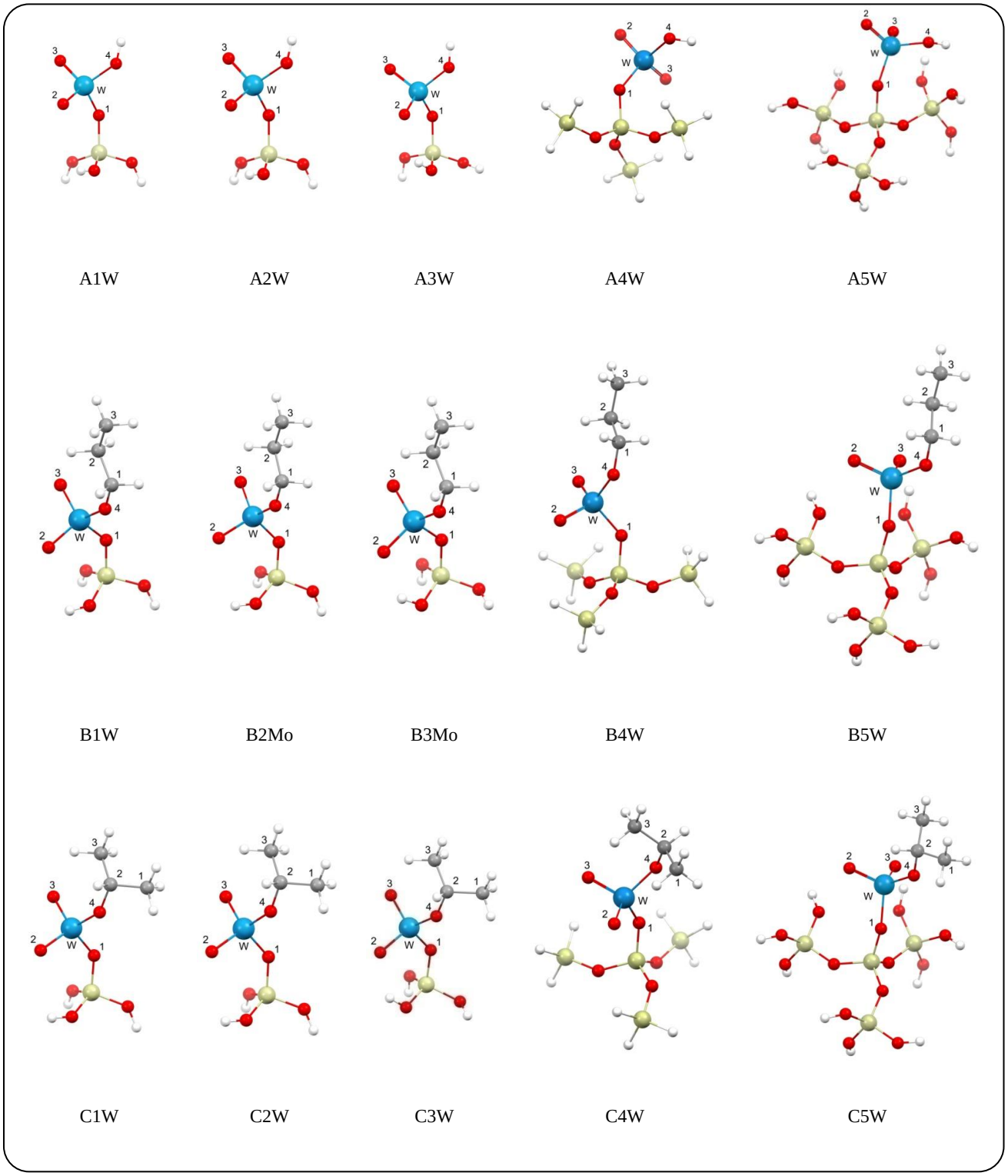

Figure S1. Continued. Optimized geometries of the original precatalyst and the resulting protonated structures after the exposure to propene on different cluster models of MoO_x/SBA-15 and WO_x/SBA-15 catalysts. The darker (red) spheres represent the framework O atoms, the plain (yellow) bigger balls are Si atoms, the plain grey spheres show C atoms, and the small white balls are terminal H atoms. The largest (blue or purple) balls represent Mo or W. Please refer to the online version for references to color

Table S1. The enthalpy (kcal/mol), entropy (kcal/mol/K), and Gibbs free energy (kcal/mol) changes for the formation of protonated products at M06/Def2-TZVP level of theory.

Product	Δ*H*	Δ*S*	Δ*G*	Product	Δ*H*	Δ*S*	Δ*G*
B1Mo	–14.64	–0.04	–2.53	B1W	–14.49	–0.04	–1.91
B2Mo	–15.46	–0.04	–3.71	B2W	–14.50	–0.04	–2.82
B3Mo	–14.69	–0.04	–3.07	B3W	–14.62	–0.04	–2.82
B4Mo	–15.81	–0.05	–1.75	B4W	–15.92	–0.05	–1.83
B5Mo	–13.78	–0.03	–4.65	B5W	–13.88	–0.03	–3.74
C1Mo	–19.18	–0.04	–7.27	C1W	–18.93	–0.04	–7.12
C2Mo	–19.06	–0.04	–7.51	C2W	–18.81	–0.04	–7.61
C3Mo	–19.16	–0.04	–7.25	C3W	–18.95	–0.04	–6.83
C4Mo	–21.04	–0.05	–7.09	C4W	–20.52	–0.05	–7.04
C5Mo	–18.67	–0.04	–6.85	C5W	–18.29	–0.04	–7.78

Table S2: Selected bonds lengths (Å) and interbond angles (in degrees) for the optimized clusters of the MoO_x/SiO_2 catalyst at the M06/Def2-TZVP level of theory.

	Bond lengths					Angles	
Cluster	Mo–O1	Mo–O4	O4–C1	O4–C2	O–H	Mo–O4–C1	Mo–O4–C2
A1Mo	1.87	1.87	—	—	0.96	—	—
A2Mo	1.87	1.87	—	—	0.96	—	—
A3Mo	1.86	1.87	—	—	0.96	—	—
A4Mo	1.88	1.87	—	—	0.96	—	—
A5Mo	1.87	1.87	—	—	0.97	—	—
B1Mo	1.87	1.85	1.41	—	—	143.0	—
B2Mo	1.87	1.86	1.41	—	—	128.6	—
B3Mo	1.87	1.85	1.41	—	—	143.9	—
B4Mo	1.88	1.85	1.41	—	—	145.4	—
B5Mo	1.87	1.86	1.41	—	—	133.1	—
C1Mo	1.87	1.85	—	1.42	—	—	143.3
C2Mo	1.87	1.85	—	1.42	—	—	143.3
C3Mo	1.87	1.85	—	1.42	—	—	143.4
C4Mo	1.88	1.85	—	1.42	—	—	138.6
C5Mo	1.87	1.86	—	1.43	—	—	129.2

Table S3: Selected bonds lengths (Å) and interbond angles (in degrees) for the optimized clusters of the WO_x/SiO_2 catalyst at the M06/Def2-TZVP level of theory.

	Bond lengths					Angles	
Cluster	W–O1	W–O4	O4–C1	O4–C2	O–H	W–O4–C1	W–O4–C2
A1W	1.88	1.88	—	—	0.96	—	—
A2W	1.88	1.88	—	—	0.96	—	—
A3W	1.87	1.88	—	—	0.96	—	—
A4W	1.89	1.88	—	—	0.96	—	—
A5W	1.88	1.89	—	—	0.96	—	—
B1W	1.88	1.86	1.41	—	—	145.9	—
B2W	1.88	1.86	1.41	—	—	145.9	—
B3W	1.87	1.86	1.41	—	—	145.8	—
B4W	1.89	1.86	1.41	—	—	146.3	—
B5W	1.88	1.86	1.41	—	—	134.6	—
C1W	1.88	1.86	—	1.42	—	—	146.8
C2W	1.88	1.86	—	1.42	—	—	146.8
C3W	1.87	1.86	—	1.43	—	—	146.8
C4W	1.89	1.86	—	1.43	—	—	140.6
C5W	1.88	1.86	—	1.43	—	—	134.6

Table S4: NBO partial charges of selected atoms and total charges (Q) of the alkoxide part on the MoO_x/SiO_2 catalyst at the M06/Def2-TZVP level of theory.

Cluster	Mo	O1	O2	O3	O4	C1	C2	C3	Q
A1Mo	1.614	–0.987	–0.485	–0.465	–0.819	—	—	—	0.505
A2Mo	1.614	–0.987	–0.485	–0.465	–0.819	—	—	—	0.505
A3Mo	1.606	–0.978	–0.511	–0.461	–0.820	—	—	—	0.506
A4Mo	1.609	–1.012	–0.457	–0.461	–0.819	—	—	—	0.508
A5Mo	1.618	–1.017	–0.457	–0.503	–0.807	—	—	—	0.505
B1Mo	1.603	–0.989	–0.499	–0.475	–0.599	–0.034	–0.419	–0.586	0.327
B2Mo	1.607	–1.002	–0.488	–0.480	–0.589	–0.046	–0.416	–0.587	0.296
B3Mo	1.595	–0.982	–0.527	–0.469	–0.600	–0.036	–0.418	–0.587	0.331
B4Mo	1.597	–1.018	–0.472	–0.472	–0.599	–0.034	–0.417	–0.587	0.333
B5Mo	1.628	–1.020	–0.469	–0.513	–0.600	–0.039	–0.411	–0.588	0.317
C1Mo	1.604	–0.991	–0.499	–0.477	–0.611	–0.601	0.120	–0.623	0.341
C2Mo	1.604	–0.991	–0.499	–0.477	–0.611	–0.601	0.120	–0.623	0.341
C3Mo	1.597	–0.986	–0.525	–0.472	–0.610	–0.601	0.120	–0.623	0.343
C4Mo	1.595	–1.017	–0.474	–0.477	–0.604	–0.618	0.118	–0.617	0.344
C5Mo	1.634	–1.024	–0.476	–0.508	–0.610	–0.599	0.112	–0.612	0.328

Table S5. NBO partial charges of selected atoms and total charges (Q) of the alkoxide part on the WO_x/SiO_2 catalyst at the M06/Def2-TZVP level of theory.

Cluster	W	O1	O2	O3	O4	C1	C2	C3	Q
A1W	1.907	–1.023	–0.599	–0.576	–0.861	—	—	—	0.510
A2W	1.907	–1.024	–0.598	–0.576	–0.861	—	—	—	0.510
A3W	1.901	–1.015	–0.625	–0.573	–0.862	—	—	—	0.512
A4W	1.899	–1.046	–0.571	–0.574	–0.858	—	—	—	0.512
A5W	1.916	–1.053	–0.571	–0.615	–0.850	—	—	—	0.506
B1W	1.891	–1.025	–0.611	–0.585	–0.644	–0.033	–0.415	–0.588	0.335
B2W	1.891	–1.027	–0.608	–0.585	–0.644	–0.033	–0.415	–0.588	0.335
B3W	1.886	–1.019	–0.638	–0.581	–0.644	–0.034	–0.416	–0.588	0.338
B4W	1.884	–1.052	–0.584	–0.585	–0.643	–0.034	–0.415	–0.588	0.339
B5W	1.916	–1.059	–0.581	–0.628	–0.640	–0.037	–0.412	–0.589	0.327
C1W	1.894	–1.029	–0.609	–0.587	–0.657	–0.602	0.124	–0.618	0.349
C2W	1.894	–1.028	–0.609	–0.587	–0.657	–0.602	0.124	–0.618	0.349
C3W	1.889	–1.020	–0.639	–0.582	–0.657	–0.602	0.123	–0.618	0.352
C4W	1.883	–1.055	–0.584	–0.589	–0.649	–0.616	0.121	–0.615	0.354
C5W	1.921	–1.059	–0.582	–0.630	–0.655	–0.601	0.119	–0.613	0.340

Table S6: Calculated HOMO and LUMO and HOMO–LUMO energy gaps ($\Delta E_{HOMO–LUMO}$) for the optimized clusters of the MoO_x/SiO_2 catalyst at M06/Def2-TZVP level of theory.

Cluster	E_{HOMO} (eV)	E_{LUMO} (eV)	$\Delta E_{HOMO–LUMO}$ (eV)
A1Mo	–8.89	–2.23	6.66
A2Mo	–8.91	–2.23	6.68
A3Mo	–9.36	–2.39	6.97
A4Mo	–9.03	–2.57	6.46
A5Mo	–8.70	–2.09	6.61
B1Mo	–8.75	–1.99	6.77
B2Mo	–8.84	–2.06	6.77
B3Mo	–8.94	–2.17	6.78
B4Mo	–8.85	–2.27	6.57
B5Mo	–8.50	–1.96	6.54
C1Mo	–8.75	–1.95	6.80
C2Mo	–8.77	–1.95	6.82
C3Mo	–8.95	–2.11	6.84
C4Mo	–8.85	–2.34	6.51
C5Mo	–8.49	–1.84	6.65

Table S7: Calculated HOMO and LUMO and HOMO–LUMO energy gaps ($\Delta E_{HOMO-LUMO}$) for the optimized clusters of the WO_x/SiO_2 catalyst at M06/Def2-TZVP level of theory.

Cluster	E_{HOMO} (eV)	E_{LUMO} (eV)	$\Delta E_{HOMO-LUMO}$ (eV)
A1W	–8.93	–1.51	7.42
A2W	–8.94	–1.51	7.43
A3W	–9.11	–1.67	7.44
A4W	–9.05	–1.83	7.22
A5W	–8.64	–1.34	7.30
B1W	–8.66	–1.30	7.36
B2W	–8.66	–1.30	7.36
B3W	–8.85	–1.44	7.41
B4W	–8.87	–1.58	7.30
B5W	–8.45	–1.27	7.17
C1W	–8.63	–1.24	7.39
C2W	–8.63	–1.24	7.39
C3W	–8.83	–1.41	7.42
C4W	–8.86	–1.65	7.21
C5W	–8.43	–1.25	7.18

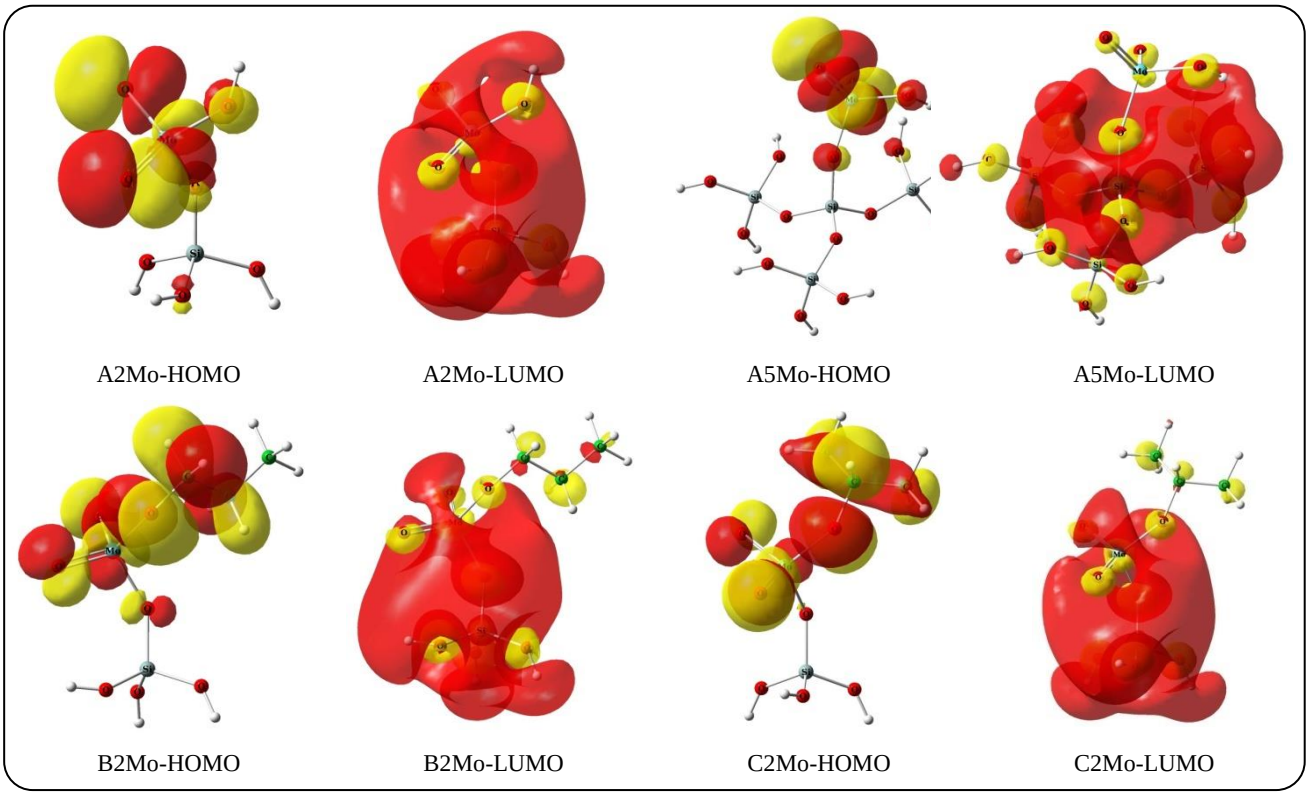

Fig. S2: Graphical presentation of molecular orbitals the original precatalyst and the resulting protonated structures after the exposure to propene on selected cluster models of MoO_x/SBA-15 and WO_x/SBA-15 catalysts.

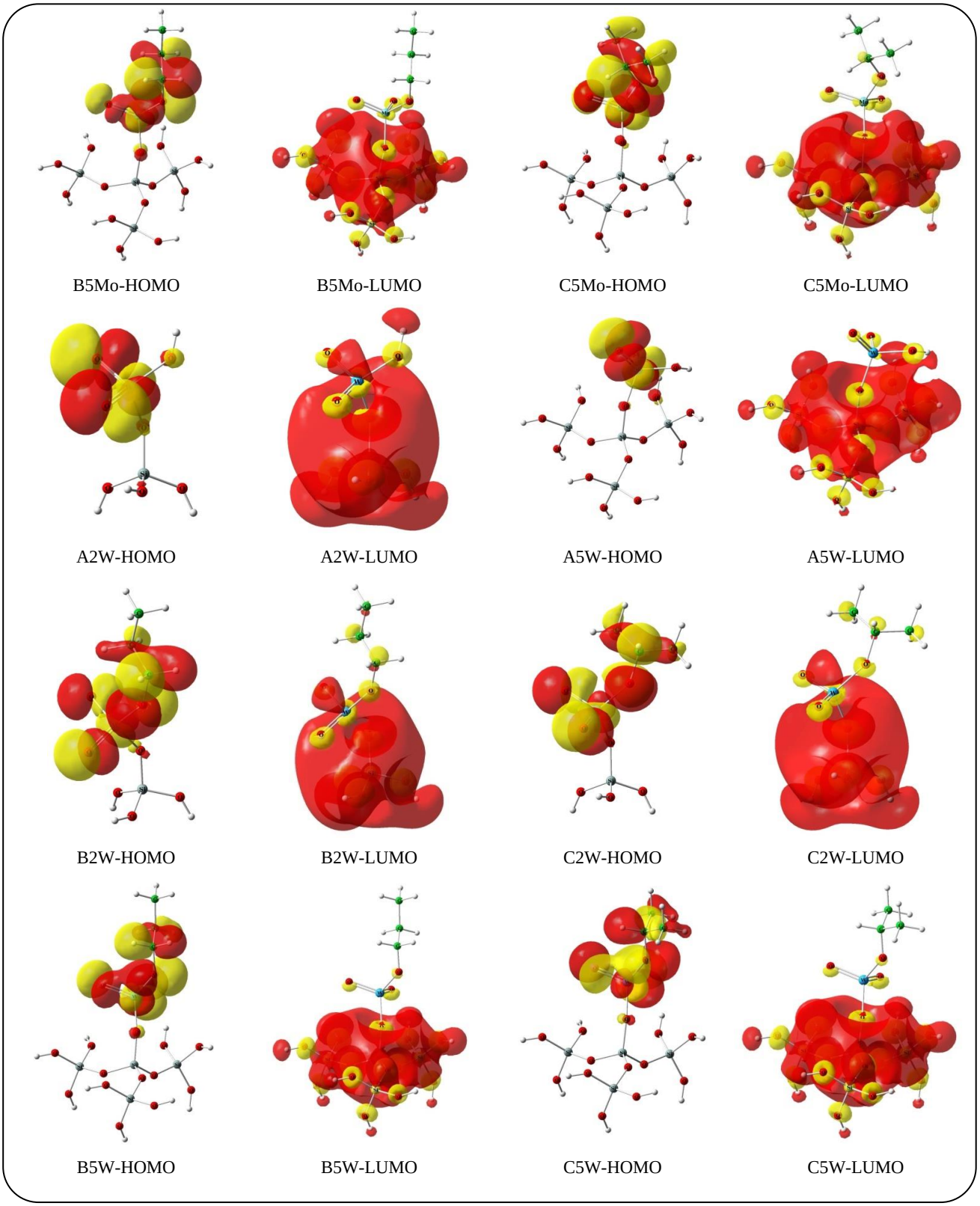

Fig. S2: Graphical presentation of molecular orbitals the original precatalyst and the resulting protonated structures after the exposure to propene on selected cluster models of MoO_x/SBA-15 and WO_x/SBA-15 catalysts. (Continued)